Available online at www.sciencedirect.com
SCIENCE DIRECT®
Journal of Catalysis 225 (2004) 267–277
JOURNAL OF CATALYSIS
www.elsevier.com/locate/jcat

Pd/CeO_2–TiO_2 catalyst for CO oxidation at low temperature: a TPR study with H_2 and CO as reducing agents

Huaqing Zhu,[a] Zhangfeng Qin,[a] Wenjuan Shan,[b] Wenjie Shen,[b] and Jianguo Wang [a,*]

[a] *State Key Laboratory of Coal Conversion, Institute of Coal Chemistry, Chinese Academy of Sciences, PO Box 165, Taiyuan, Shanxi 030001, People's Republic of China*

[b] *State Key Laboratory of Catalysis, Dalian Institute of Chemical Physics, Chinese Academy of Sciences, PO Box 110, Dalian, Liaoning 116023, People's Republic of China*

Received 2 January 2004; revised 31 March 2004; accepted 9 April 2004

Available online 20 May 2004

Abstract

The catalysts Pd/TiO_2, Pd/CeO_2, and Pd/CeO_2–TiO_2 for CO oxidation at low temperature together with their corresponding supports TiO_2, CeO_2, and CeO_2–TiO_2 prepared by sol–gel precipitation followed by supercritical fluid drying were characterized by means of N_2 adsorption, XRD, diffuse reflectance infrared Fourier transform spectroscopy (DRIFTS) of CO adsorption and temperature-programmed reduction (TPR) with H_2 and CO as reducing agents. The results showed that PdO is finely dispersed on the supports with high surface area. DRIFTS of CO adsorption further indicated that both Pd^{2+} and Pd^0 species coexist in Pd/CeO_2, while only Pd^0 is detected in Pd/TiO_2 and Pd/CeO_2–TiO_2. H_2-TPR showed that no bulk CeO_2 exists in CeO_2–TiO_2 and the reduction of CeO_2–TiO_2 is more difficult than that of the surface oxygen in the individual CeO_2 probably due to the formation of CeO_2–TiO_2 solid solution. PdO in Pd/TiO_2 can be fully reduced by H_2 at ambient temperature, whereas PdO in Pd/CeO_2 and Pd/CeO_2–TiO_2 is reduced respectively at 162 and 80 °C, accompanied by the reduction of surface CeO_2. CO-TPR showed that the reduction of PdO in PdO/TiO_2 is limited within the outermost layer at ambient temperature and the core PdO can only be reduced with a further increase of temperature. PdO/CeO_2 is also reduced both at ambient temperature and with the increase of temperature during the CO-TPR process, and the reduction temperature of CeO_2 decreased significantly in the presence of PdO, which may be due to the different degrees of interaction between PdO and CeO_2. In contrast, a complete reduction of PdO in Pd/CeO_2–TiO_2 by CO is observed at ambient temperature, accompanied by the partial reduction of CeO_2, which may indicate that the special Pd–Ce–Ti interaction in Pd/CeO_2–TiO_2 is favorable for the reduction of PdO and interfacial CeO_2 species. The water–gas shift (WGS) between CO and the hydroxyl groups in the catalysts is detected at a temperature higher than 210 °C on all of the Pd-supported catalysts as well as the individual CeO_2 and TiO_2 supports.

Keywords: CO oxidation; Ceria; Titania; Palladium; Temperature-programmed reduction

1. Introduction

The catalytic oxidation of CO has attracted considerable attention due to the increasing applications in the automotive emission control, trace CO removal in the enclosed atmospheres, and carbon dioxide lasers exhaust abatement. Catalysts containing noble metals such as Au [1–6], Pt [7,8], and Pd [9–12] have been proved very effective for CO oxidation at low temperature. Pd supported catalysts have drawn much attention due to the excellent activity for the low-temperature oxidation of CO and hydrocarbons compared with Pt and Rh-supported catalysts [13] and the theoretical significance for the interpretation of the metal–support interaction.

Since Tauster et al. reported the strong metal–support interaction (SMSI) [14], a great deal of effort has been devoted to this subject [15]. The SMSI reported for M/TiO_2 after reduction at high temperatures has been attributed to both electronic and geometric effects (metal decorations). Although there is still some disputation, the TiO_2-based noble metal catalysts exhibited significantly high activities for the methane or methanol synthesis from syngas due to the SMSI effect [16,17]. Au supported on TiO_2 showed high ac-

* Corresponding author. Fax: +86 351 4041153.
E-mail address: iccjgw@sxicc.ac.cn (J. Wang).

0021-9517/$ – see front matter
doi:10.1016/j.jcat.2004.04.006

tivity for CO oxidation even at relatively low temperatures due to the synergistic effect between gold and TiO_2 support [18]. Kochubey et al. [9] and Pavlova et al. [10,11] reported that the CO oxidation at room temperature over Pd supported on TiO_2, SiO_2, and γ-Al_2O_3 was structure-sensitive and proceeded via the interaction between weakly bounded CO and oxygen located at the defect centers [9–11].

Recently, there has been great interest in the use of ceria as a promoter in the three-way catalysis since it was suggested to improve the noble metal dispersion and the thermal stability of support alumina, to enhance the activity of CO oxidation and water–gas shift reaction, and to improve the ability of oxygen storage and releasing [19,20]. Fernández-García et al. investigated the CO oxidation performance of Pd supported on Al_2O_3, CeO_2, and CeO_2–Al_2O_3 [21]; ceria facilitated the activation of CO and oxygen respectively through the promoted formation of metallic Pd and the presence of reactive vacancies at the Pd–Ce interface. For the catalysts of precious metals supported on ceria, temperature-programmed desorption (TPD) of the adsorbed CO has shown that CO adsorbed on the metals can reacted with oxygen from the support ceria [22–24]. This ceria-mediated process can also lead to large enhancements of reaction rate for the steady-state CO oxidation [25–29]. The ceria loaded with platinum is also an effective catalyst for the water–gas shift (WGS). Bunluesin and Gorte [30] studied the kinetics over ceria-supported Pt, Rh, and Pd and proposed a redox reaction mechanism, whereby CO adsorbed on the precious metal is oxidized by ceria which in turn is oxidized by water. Both the ceria-mediated CO oxidation and WGS appear to be controlled by two steps: the transfer of oxygen from ceria to the metal interface and the reaction rate of ceria reoxidation. Therefore, the oxygen-storage capacity and oxygen mobility in such catalyst are very important, which usually can be determined by temperature-programmed reduction (TPR) with H_2.

In our previous work [31], Pd supported over ceria–titania mixed oxides prepared by sol–gel precipitation followed by supercritical fluid drying (SCFD) exhibited high activity for CO oxidation at low temperatures. Pd/CeO_2–TiO_2 was more active than Pd/CeO_2 and Pd/TiO_2; with a Pd loading of 1.0 wt% and the mole ratio of titania to ceria ranging from 7 to 5, CO in the stream (0.57 vol% CO, 1.5 vol% O_2, balance Ar, and GHSV $= 3\text{–}4 \times 10^4\ h^{-1}$) could be fully converted to CO_2 at ambient temperature over 8 h without any deactivation. The objective of this work is to gain insight into the roles of Pd active species and the surface oxygen of reducible supports in the CO oxidation at low temperatures, to elaborate the Pd–support interaction and the variation of catalytic activity of different catalysts, and then to correlate the catalytic behaviors with the preparation parameters and pretreatment of the catalysts. As a consequence, the catalysts Pd/TiO_2, Pd/CeO_2, and Pd/CeO_2–TiO_2 for CO oxidation at low temperature together with their corresponding supports TiO_2, CeO_2, and CeO_2–TiO_2 were characterized by means of N_2 adsorption, X-ray diffraction (XRD), diffuse reflectance infrared Fourier transform spectroscopy (DRIFTS) of CO adsorption, and TPR with H_2 and CO as reducing agents.

2. Experimental

2.1. Catalyst preparation

The CeO_2, TiO_2, and CeO_2–TiO_2 supports were prepared by sol–gel precipitation followed by SCFD, as described elsewhere [31]. Briefly, a hydrosol of titanium hydroxide was obtained through the hydrolysis of $TiCl_4$, then the aqueous solution of $Ce(NO_3)_3 \cdot 6H_2O$ was added under stirring. The precipitation was achieved with the concentrated ammonia solution at ambient temperature. After aging, washing, and exchanging water with ethanol, the wet precipitate was dried with supercritical ethanol and finally calcined at 500 °C in air for 3 h. The individual TiO_2 and CeO_2 supports were also prepared in a similar way. Pd supported catalysts were prepared through incipient wetness impregnation at ambient temperature with aqueous $PdCl_2$ solution as Pd precursor. The catalysts were then dried at 120 °C for 20 h and calcined at 500 °C for 3 h. The mole ratio of titania to ceria is 5 for the CeO_2–TiO_2 support, and the Pd loading is 1 wt% for the Pd supported catalysts.

2.2. Catalyst characterization

The surface area and textural properties of the catalysts were measured by nitrogen adsorption at 77.4 K with ASAP2000 (Micromeritics Instrument Co., USA). The catalyst samples were degassed at 200 °C and 6.7 Pa for 4–5 h prior to the measurement.

XRD characterization of the catalyst samples was preformed on a Rigaku D/max-2500 X-ray diffraction spectrometer. The diffraction patterns were recorded at room temperature using Cu-K_α radiation (0.15418 nm, 40 KV, and 100 mA). The average crystallite size was determined from the diffraction peak broadening with the Scherrer formula [32].

DRIFTS of CO adsorption was measured with a Vector 22 spectrometer (Bruker) equipped with a DTGS detector, and the cell was fitted with ZnSe windows and a heating chamber allowed samples to be heated up to 900 °C. The DRIFTS spectra were obtained from single beam spectra with a resolution of 4 cm^{-1} recorded against a background spectrum of the sample purified just prior to introducing the adsorbates and 50 scans were taken to improve the signal-to-noise level. Approximately 40 mg sample was used per run. The sample was purified in a He (99.999%) flow of ca. 30 ml/min at 500 °C for 1 h and cooled down to 25 °C, then exposed to the flow of 5.01% CO in Ar (ca. 30 ml/min) to a saturated adsorption and flushed with He flow again. The spectra of CO adsorption at 25 °C after purging with He flow were then recorded. The spectra of CO adsorption with the

sample being exposed to the CO/Ar flow were also recorded at different temperatures.

H_2-TPR was performed in a quartz microreactor, and about 50 mg sample was used in each measurement. The samples were first pretreated under an air flow at 500 °C for 1 h, followed by purging with N_2 at the same temperature for 1 h and cooling down to room temperature. The flow of 6% H_2 in N_2 (30 ml/min) was then switched into the system, and the sample was heated up to 820 °C from room temperature at a rate of 10 °C/min. The amount of H_2 uptake during the reduction was measured by a thermal conductivity detector (TCD), which was calibrated by the quantitative reduction of CuO to the metallic copper.

CO-TPR was operated in the same way as H_2-TPR excepting that the purge gas was Ar instead of N_2 and the reducing agent was 2% CO in Ar. CO-TPR was then conducted from room temperature to 500 °C at a heating rate of 10 °C/min. CO, CO_2, and H_2 in the outlet gas were measured by a mass spectrometer OmniStar equipped with the software Quadstar 32-bit. The intensity of CO and H_2 signals is calibrated by using CO(2%)/Ar and H_2(6%)/N_2, respectively. CO_2 signal is calibrated by the pulse of pure CO_2 with an eight-port pulsing valve. The uptakes of CO and the amounts of CO_2 and H_2 evolved during the measurement were then determined from the mass signals and the flow rate (30 ml/min) of reducing agent.

3. Results and discussion

3.1. Surface area and textural structure

The BET surface area and the textural structure of Pd/CeO_2, Pd/TiO_2 and Pd/CeO_2–TiO_2 are listed in Table 1. Pd/TiO_2 exhibits a comparable surface area with Pd/CeO_2, but with larger pore volume and average pore size than Pd/CeO_2. However, the surface area and pore volume of Pd/CeO_2–TiO_2 are much larger than those of both Pd/TiO_2 and Pd/CeO_2, which may contribute to the high activity for the CO oxidation at low temperature.

3.2. XRD

The XRD patterns of Pd/CeO_2, Pd/TiO_2, and Pd/CeO_2–TiO_2 catalysts are shown in Fig. 1. Cerianite and anatase phases are observed in Pd/CeO_2 and Pd/TiO_2, respectively. In the case of Pd/CeO_2–TiO_2, the anatase phase is still present, but the cerianite phase is replaced by an amorphous phase with two broad peaks. The PdO phase is not observed in all the samples, indicating that either PdO is present as a noncrystalline phase or the particle size is smaller than 3 nm and finely dispersed on the supports.

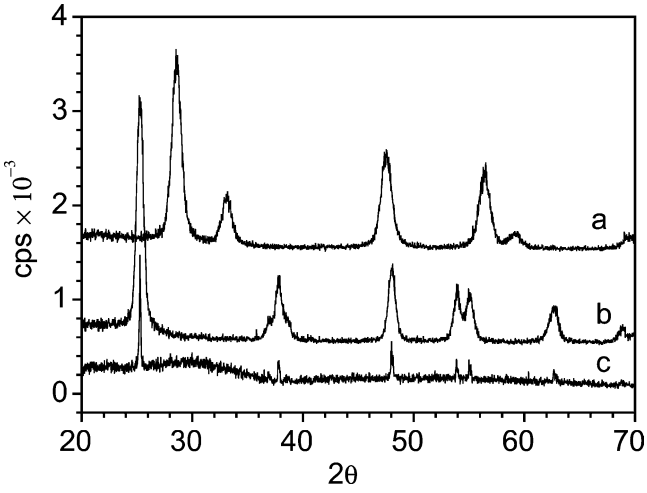

Fig. 1. XRD patterns of the calcined catalysts (a) Pd/CeO_2, (b) Pd/TiO_2, and (c) Pd/CeO_2–TiO_2.

The crystal sizes of CeO_2 in Pd/CeO_2 and TiO_2 in Pd/TiO_2 calculated from cerianite (111) plane and anatase (101) plane are 7 and 10 nm, respectively, while the crystal size of TiO_2 in Pd/CeO_2–TiO_2 is approximately 30 nm from the calculation of anatase (101) plane. Dong et al. [33] found that the large crystallite anatase particles in the mixed oxide were originated from the SCFD of gel during the preparation process. The XRD patterns indicated that Ce^{3+} ions do not incorporate into the lattice of TiO_2 to replace the Ti^{4+} ions in the large crystallites because the ionic radii of Ce^{4+} (0.993 Å) is much larger than that of Ti^{4+} (0.68 Å) [34]. Thus, it is concluded that two kinds of particles are present in the CeO_2–TiO_2 support: the TiO_2-rich anatase phase with large particle size of 30 nm and CeO_2-rich amorphous phase with fine particles. Moreover, the fine particles could be a solid solution of CeO_2–TiO_2 with good thermal stability and are able to endure the calcination at 500 °C, which is consistent with those reported by Dauscher et al. [35], Luo et al. [36], and Rynkowski [37].

3.3. DRIFTS of CO adsorption

The DRIFTS spectra of CO adsorbed at 25 °C on Pd/CeO_2, Pd/TiO_2, and Pd/CeO_2–TiO_2 are shown in Fig. 2. For all the samples, the band in the region of 2300–2400 cm^{-1} is

Table 1
Surface area and pore structure of the catalysts

Catalyst	Surface area (m^2/g)	Pore volume (cm^3/g)	Average pore size (nm)	Compounds identified by XRD
Pd/TiO_2	95.9	0.3	14	Anatase
Pd/CeO_2	89.0	0.2	7	Cerianite
Pd/CeO_2–TiO_2	167.3	0.5	12	Anatase, amorphous

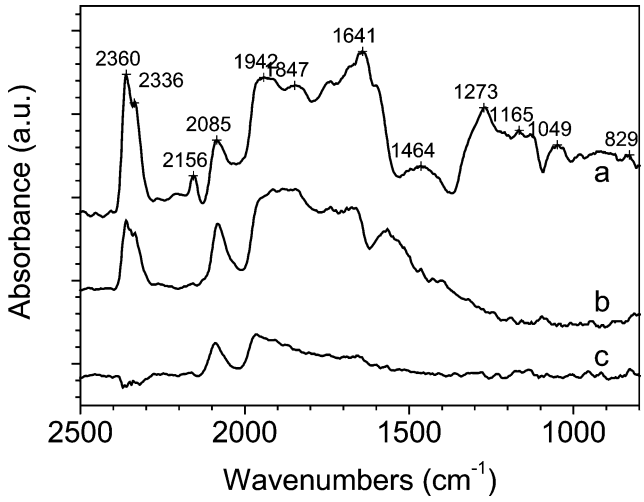

Fig. 2. DRIFTS of CO adsorption at 25 °C on (a) Pd/CeO_2, (b) Pd/TiO_2, and (c) Pd/CeO_2–TiO_2 after purging with He for 15 min.

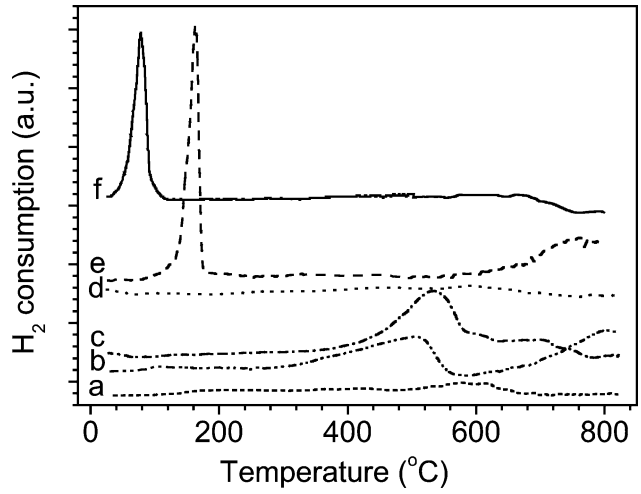

Fig. 3. H_2-TPR profiles of (a) TiO_2, (b) CeO_2, (c) CeO_2–TiO_2, (d) Pd/TiO_2, (e) Pd/CeO_2, and (f) Pd/CeO_2–TiO_2.

assigned to the gaseous CO_2. For the Pd/CeO_2 catalyst, the peaks at 2156 and 2085 cm^{-1} are ascribed to the linear adsorption of CO on Pd^{2+} and Pd^0, respectively [21,38–41]. The asymmetrical broad band at 1940 cm^{-1} is attributed to the bridge adsorption of CO on Pd^0 sites. The initial Pd species should be in the form of PdO (Pd^{2+}), because the fresh catalyst was calcined in air at 500 °C for 3 h. The appearance of Pd species in lower valence indicates that Pd^{2+} in the calcined catalyst has been partially reduced by CO at ambient temperature. The linear bond of CO on Pd^+ at 2110 cm^{-1} was not detected, indicating that Pd^{2+} may be directly reduced to metallic palladium by CO rather than through the intermediate Pd^+. The weak bands in the region of 1800–800 cm^{-1} should be assigned to the carbonate-like species formed on CeO_2 support [42,43].

The DRIFTS spectra of CO adsorbed on Pd/TiO_2 at 25 °C exhibit a linear adsorption of CO on metallic Pd at 2081 cm^{-1}. The bridged bond of CO with Pd atoms was also observed below 2000 cm^{-1}. The Pd^{2+}/Pd^+ species (linear adsorption at 2158 cm^{-1} for Pd^{2+} and 2110 cm^{-1} for Pd^+) were not detected, indicating that the surface PdO has been completely reduced to Pd^0. No band for the carbonate-like species was detected in the region of 1800–1000 cm^{-1}.

For Pd/CeO_2–TiO_2, the DRIFTS spectra of CO adsorption show that PdO in the calcined Pd/CeO_2–TiO_2 has been completely reduced to Pd^0 (linear adsorption at 2189 cm^{-1} and bridged adsorption at 1965 cm^{-1}). It should be noted that the intensity of the adsorbed CO on Pd/CeO_2–TiO_2 is much lower than those on Pd/CeO_2 and Pd/TiO_2. This may suggest that the interaction of adsorbed CO with Pd in Pd/CeO_2–TiO_2 is much weaker. Like the spectra for Pd/TiO_2, there were also no carbonate-like species detected in the region of 1800–1000 cm^{-1}. It should be noted that the catalysts Pd/CeO_2, Pd/TiO_2, and Pd/CeO_2–TiO_2 are different in the exact band positions of the linear adsorption on metallic Pd, which may imply that they are also different in the electronic effects of metal–support interaction.

3.4. H_2-TPR

The H_2-TPR profiles of Pd/CeO_2, Pd/TiO_2, and Pd/CeO_2–TiO_2 along with the corresponding supports are shown in Fig. 3.

H_2-TPR of individual TiO_2 shows two poorly identified peaks at 575 and 615 °C, respectively. However, the reduction of Pd/TiO_2 takes place immediately after the H_2/N_2 flow was switched into the system at ambient temperature and no evident TPR peak is observed excepting a small broad peak at ca. 600 °C that may be ascribed to the reduction of TiO_2 support. These suggest that PdO in Pd/TiO_2 can be fully reduced by the diluted H_2 at ambient temperature.

H_2-TPR has been extensively used to characterize the reducibility of oxygen species in CeO_2 and CeO_2 containing materials. It was found that the reduction peaks of the surface-capping oxygen and the bulk oxygen of CeO_2 were centered at 500 and 800 °C, respectively [44]. The reduction of ceria depended strongly on the ceria crystallite size [19,45], and the oxygen migration in Rh/ceria catalyst was significantly affected by the structure of ceria [46]. For the H_2-TPR of CeO_2 in this work, the reduction of CeO_2 starts at 280 °C and two broad peaks are observed at 510 and 800 °C, respectively. The peak at 510 °C, which was assigned to the reduction of surface-capping oxygen of ceria [44], corresponds to a H_2 consumption of 1153 μmol/g, as listed in Table 2. The peak at 800 °C can be ascribed to the reduction of bulk CeO_2 with a H_2 uptake of 1702 μmol/g. Stoichiometrically, 1 g CeO_2 requires 2905 μmol H_2 for a complete reduction by assuming the following reduction process

$$2CeO_2 + H_2 \rightarrow Ce_2O_3 + H_2O.$$

Therefore, CeO_2 is almost totally reduced at 820 °C with a H_2 consumption of 2855 μmol/g and the proportion of CeO_2 reducible at low temperatures (280–560 °C) is approximately 40% with a H_2 consumption of 1153 μmol/g. Such a H_2 consumption at low temperatures corresponds to

Table 2
H_2-TPR and CO-TPR results

Sample[a]	CeO_2 content (μmol/g)	H_2 uptake[b] (μmol/g)		CO_2 evolved[c] (μmol/g)		Reducible CeO_2[d] (%)	
		Low	High	RT	TPR	H_2-TPR	CO-TPR
CeO_2	5810	1153	1702			40	
CeO_2–TiO_2	1750	870				100	
Pd/TiO_2	–	–	–	18	64	–	–
Pd/CeO_2	5752	1250	1685	71	776	40	26
Pd/CeO_2–TiO_2	1732	965	–	123	805	100	96

[a] The mole ratio of TiO_2 to CeO_2 is 5 for the support CeO_2–TiO_2; Pd loading is 1 wt% (94 μmol/g) for the Pd-supported catalysts.
[b] "Low" and "High" represent respectively the low and high temperature band in H_2-TPR profiles shown in Fig. 3.
[c] The amounts of CO_2 evolved at room temperature (RT) were calculated according to the corresponding curves shown in Fig. 6, and those during CO-TPR process were calculated from the corresponding curves shown in Fig. 7 for Pd/CeO_2, Fig. 10 for Pd/TiO_2, and Fig. 13 for Pd/CeO_2–TiO_2, respectively.
[d] For the H_2-TPR, the reducible CeO_2 is the proportion of H_2 uptake at low temperature (with the deduction of the H_2 uptake due to the PdO reduction in the case of Pd-supported catalysts). For the CO-TPR, the reducible CeO_2 = 2(total amounts of CO_2 evolved − CO_2 evolved due to reduction of PdO − H_2 production)/CeO_2 content.

5.0×10^{18} oxygen/m^2 (the BET area of ceria used in this work is 137 m^2/g), which implies significant bulk reduction besides the surface reduction. This may be due to that the oxygen transfer and reduction are enhanced by the grain boundaries and defects in the small ceria crystallites (about 70 Å) [46].

H_2-TPR of Pd/CeO_2 shows two reduction peaks at 162 and 770 °C, respectively. The peak at 770 °C with a H_2 consumption of 1685 μmol/g is ascribed to the reduction of lattice oxygen in bulk CeO_2, while the peak at 162 °C with a H_2 consumption of 1250 μmol/g is assigned to the reduction of the species related to the PdO–CeO_2 interaction. Stoichiometrically, the H_2 consumption for the reduction of PdO to Pd is 94 μmol/g for the catalysts with a Pd loading of 1 wt%, i.e.,

$$PdO + H_2 \rightarrow Pd + H_2O.$$

The H_2 consumption due to the reduction of both PdO (94 μmol-H_2/g) and the proportion of CeO_2 reducible at low temperatures (1153 μmol-H_2/g) contribute simultaneously to the reduction peak at 162 °C (1250 μmol-H_2/g), which suggests that PdO is well-dispersed on the support and only part of CeO_2 interacts with PdO. Such results are also consistent with the general considerations that the reduction temperature of PdO in Pd/CeO_2 shifts to a higher value compared with the individual PdO, while the reduction temperature of CeO_2 in Pd/CeO_2 is lower than that of individual CeO_2, due to the interaction between PdO and CeO_2 [12,47].

H_2-TPR profile of CeO_2–TiO_2 exhibits one broad reduction band that starts at 370 °C with a maximum at 530 °C, followed by a small shoulder at 613 °C. Compared with the H_2-TPR profiles of individual TiO_2 and CeO_2, the small shoulder at 613 °C should be assigned to the reduction of TiO_2, while the band at 530 °C should be ascribed to the reduction of CeO_2. The increase of the reduction temperature indicates that CeO_2 in CeO_2–TiO_2 support becomes much more difficult to be reduced due to the possible formation of a CeO_2–TiO_2 solid solution. There is no evident reduction of bulk CeO_2 at high temperatures as opposed to the individual CeO_2; the H_2 consumption corresponding to the reduction of CeO_2 is 870 μmol/g, which is close to the stoichiometrical amounts of H_2 (875 μmol/g) necessary for a complete reduction of CeO_2 in CeO_2–TiO_2. These may suggest that no bulk CeO_2 species exist in the mixed oxides support, which is in accordance with the results of XRD.

For Pd/CeO_2–TiO_2, H_2-TPR gives one single sharp peak at about 80 °C with the H_2 consumption of 965 μmol/g, which can be assigned to the reduction of both PdO (94 μmol-H_2/g) and CeO_2 (875 μmol-H_2/g). The reduction temperature of CeO_2 decreases greatly due to the Pd–Ce interaction in Pd/CeO_2–TiO_2, although the reduction of CeO_2 in CeO_2–TiO_2 in the absence of Pd is much more difficult compared with the individual CeO_2.

3.5. CO-TPR

Although CO was rarely used as reducing agent in the TPR characterization compared with H_2, CO-TPR is one of the best probes to investigate the reducibility of both the PdO and the supports for CO-involved reactions and is helpful to identify the surface oxygen species and the finely dispersed PdO [12,48,49].

During the CO-TPR process, H_2 and CO_2 are formed with the consumption of CO. H_2 and CO_2 may be produced from the water–gas shift due to the interaction of CO with the hydroxyl groups in the catalysts

$$CO(ads) + 2OH^-(support) \rightarrow CO_2(g) + H_2(g) + O^{2-}(support).$$

CO_2 is also formed through either the reduction of reducible species such as PdO and CeO_2,

$$CO + PdO \rightarrow Pd + CO_2,$$

$$CO + 2CeO_2 \rightarrow Ce_2O_3 + CO_2,$$

or the disproportionation of CO

$$2CO \rightarrow CO_2 + C,$$

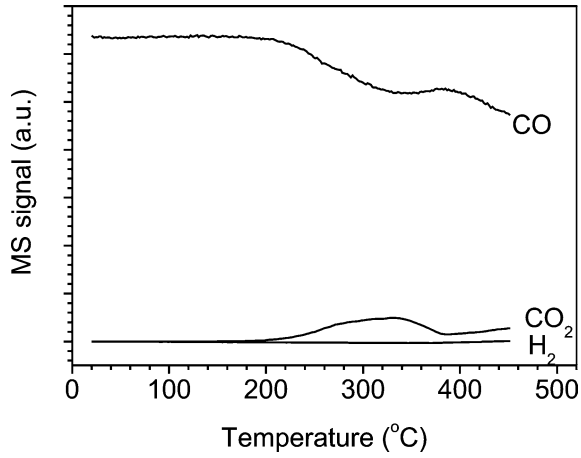

Fig. 4. CO-TPR profiles of reference sample (1% Pd supported on quartz sand).

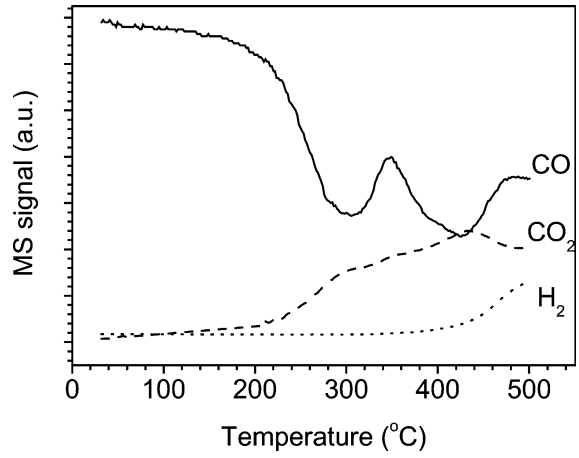

Fig. 5. CO-TPR profiles of the calcined CeO_2.

which would lead to carbon deposition on the catalyst surface. On the other hand, the formation of carbonate species at certain circumstance will also cause the consumption of CO, while the decomposition of carbonate species will contribute to the evolution of CO_2.

In order to investigate the behaviors of CO-TPR of different catalysts, a blank test was first carried out on quartz sand with 1 wt% Pd loading, as shown in Fig. 4. CO_2 is formed from about 200 °C and peaks at 330 °C with the consumption of CO. The CO_2 production should be ascribed to the reduction of bulk PdO. No H_2 formation is detected during the TPR process. The amount of CO_2 produced is 56.6 μmol/g, which accounts for 60% PdO in the sample. This may suggest that the reduction of bulk PdO is stepwise by CO.

3.5.1. *CeO_2 and Pd/CeO_2*

For the CO-TPR of CeO_2, as shown in Fig. 5, two CO consumption peaks are observed at 305 and 425 °C, respectively. The production of CO_2 shows two peaks at 310 °C (shoulder) and 430 °C, respectively. H_2 emission starts at 350 °C and becomes significant at temperatures higher than 450 °C. Because the bulk CeO_2 can only be reduced at a temperature higher than 500 °C as revealed by H_2-TPR, the CO_2 evolved between 200 and 500 °C should be attributed to the reduction of lattice oxygen on the CeO_2 surface and/or the WGS reaction.

To check whether the CO disproportionation occurred, the sample after the CO-TPR process is purged with Ar flow and then subjected to an O_2-TPO from room temperature to 500 °C in a O_2(2.5%)/Ar flow. No evident O_2 consumption is detected during the heating; however, a large amount of CO_2 is detected at a temperature above 400 °C. This may suggest that Ce_2O_3 formed during the CO-TPR has been oxidized to CeO_2 at room temperature, since the oxidation of Ce_2O_3 by O_2 is known to occur at such a low temperature. The release of CO_2 at high temperature without any O_2 consumption should be assigned to the decomposition of carbonate species on ceria. Because no O_2 is consumed due to the oxidation of deposited C, the CO disproportionation during the CO-TPR of CeO_2 is negligible under the present conditions. This is consistent with the results reported by Serre et al. [48] and Martínez-Arias et al. [49].

The production of H_2 is related to the WGS reaction between the CO and the hydroxyl groups in the sample. The suggestion is confirmed by the second TPR process after O_2-TPO, where the peaks of H_2 signals were weakened due to the diminishing of the hydroxyl groups in the sample. The same phenomena were also found by Serre et al. [48], where the consumption of CO and simultaneous formation of CO_2 at temperatures above 400 °C during the CO-TPR of γ-alumina were assigned to the reaction of gaseous CO with the hydroxyl groups remaining on the alumina surface. Martínez-Arias et al. [49] detected the H_2 formation during the CO-TPR on CeO_2/Al_2O_3, Pt/Al_2O_3, and $Pt/CeO_2/Al_2O_3$, indicating the onset of the WGS reaction.

Therefore, the CO-TPR patterns may be associated with the formation of various nonstoichiometrical cerium oxide species. It is interesting that CO can reduce the surface CeO_2 even at a lower temperature compared with H_2 as the reducing agent, although it is generally considered that CO is a weaker reducing agent than H_2. The reason may be that the dissociation of adsorbed H_2 is necessary for the reduction by H_2, while CO can directly attack the surface oxygen in CeO_2 sample.

For the CO-TPR of Pd/CeO_2, CO_2 is first released at ambient temperature (see Fig. 6 and Table 2), which can be ascribed to the reduction of PdO. With the increase of temperature (see Fig. 7), the CO_2 production shows three peaks with apexes at 70, 220 (as a shoulder), and 360 °C, respectively. The amount of CO_2 evolved at ambient temperature is 71 μmol/g, which indicates that the reduction of PdO is not completed at ambient temperature, because the CO_2 production will be 94 μmol/g for a complete reduction. The peak at 70 °C should be assigned to the reduction of both PdO and CeO_2, which presents likely as an interfacial species;

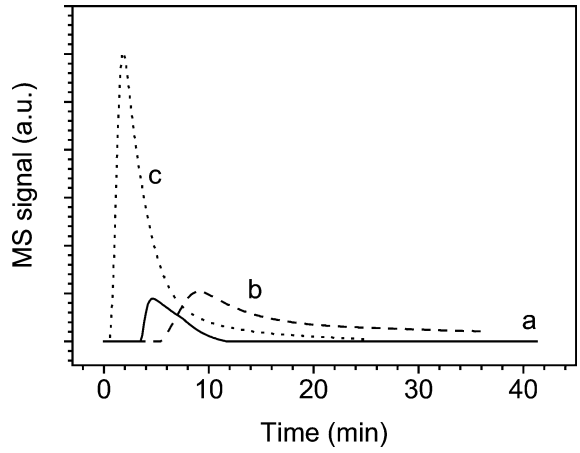

Fig. 6. Amounts of CO_2 evolved in CO-TPR at ambient temperature on (a) Pd/TiO_2, (b) Pd/CeO_2, and (c) Pd/CeO_2–TiO_2.

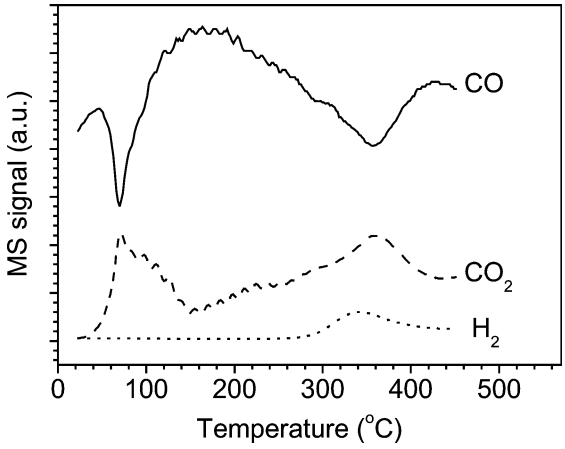

Fig. 7. CO-TPR profiles of the calcined Pd/CeO_2.

the CO_2 production above 150 °C should be attributed to the reduction of lattice oxygen on the CeO_2 surface. In the successive O_2-TPO process, a large amount of CO_2 is released at a temperature above 370 °C without evident O_2 consumption, which confirms that the CO disproportionation in the CO-TPR process is negligible and the CO_2 formation in O_2-TPO is originated from the decomposition of carbonates. Compared with the individual CeO_2, the interaction between Pd and CeO_2 lowers the reduction temperature of CeO_2, which is consistent with the result of H_2-TPR. The H_2 formation starts at 270 °C and reaches a maximum at about 340 °C due to the WGS reaction between the adsorbed CO and the hydroxyl groups on the support. This was confirmed by the second CO-TPR after O_2-TPO: the signal of H_2 was decreased due to the diminution of the hydroxyl groups during the first TPR. The reproduction of the CO-TPR profiles is obtained when the sample was exposed to the water vapor at 120 °C, indicating that the hydroxyl groups and then the WGS reactivity can be restored.

DRIFTS of CO adsorption indicates that Pd^{2+} and Pd^0 coexist in Pd/CeO_2 catalyst (see Fig. 2). The variance of the PdO reducibility in Pd/CeO_2 should be from the different ways of PdO–CeO_2 interaction or different orientations of PdO combined to the support. The easily reducible Pd^{2+} that can be reduced at ambient temperature may locate on the outermost surface of PdO–CeO_2, while the band at higher temperatures (32–150 °C, peaked at 70 °C) involves the reduction of both PdO and CeO_2, which is most likely due to the formation of a kind of PdO–CeO_2 interfacial species.

The WGS on ceria-based catalysts is thought to proceed mainly through the regenerative (redox) mechanism and the associative mechanism. The regenerative mechanism involves successive oxidation and reduction of the surface, while the associative mechanism involves reaction through an adsorbed surface intermediate. Bunluesin et al. have recently proposed a mechanism that involves a ceria-mediated redox process, whereby CO adsorbed on the precious metal is oxidized by ceria that in turn is oxidized by water [30]. Shido and co-workers [50,51] investigated the catalytic WGS on Rh-doped CeO_2 by using TPD and infrared spectroscopy and found that the intermediate for the reaction is a bidentate formate which is produced by the reaction of CO with terminal surface hydroxyl groups on Ce ions. The rate-determining step is the decomposition of the bidentate formate to H_2 and a unidentate carbonate. The IR studies reported by Jacobs et al. also favor the bidentate formate mechanism in explaining the WGS reaction on Pt/CeO_2 [52].

In order to examine the intermediates formed here during the CO-TPR, the DRIFTS are carried out with the sample being exposed to CO (5.01%) in Ar at different temperatures. As shown in Fig. 8, the spectrum at 25 °C shows that the bands located at 2358 and 2336 cm^{-1} are ascribed to the absorbance of gaseous CO_2. The bands at 2158 and 2100 cm^{-1} overlapped by the absorption of gaseous CO are ascribed to the linearly CO adsorbed on Pd^{2+} and Pd^0, respectively, while the band at 1940 cm^{-1} is assigned to the bridged bond CO on Pd^0 as discussed above. The carbonate-like species are detected at room temperature in the region of 1800–800 cm^{-1}. With the increase of temperature, the carbonates remain in the sample. However, when the temperature increased to about 200 °C, the negative band located at 3642 and 3665 cm^{-1} assigned to the geminal OH groups on Ce ions appears, indicating the decrease of OH groups. Simultaneously, the bands at 2943 and 2860 cm^{-1} were detected, which should be assigned to the absorption of bidentate formate species on Ce ions [42,53]. With the further increase of temperature, OH groups are continuously decreased and the formate species are constantly increased accompanied with an increase of the carbonate species. Therefore, we suggest that WGS here follows the associative mechanism: the adsorbed CO on Pd reacts with the geminal hydroxyl groups on ceria to form bidentate formate species, and the formate decomposition will give carbonate and H_2.

3.5.2. *TiO_2 and Pd/TiO_2*

For the CO-TPR of individual TiO_2, a small amount of CO_2 is released from 310 °C accompanied with H_2 for-

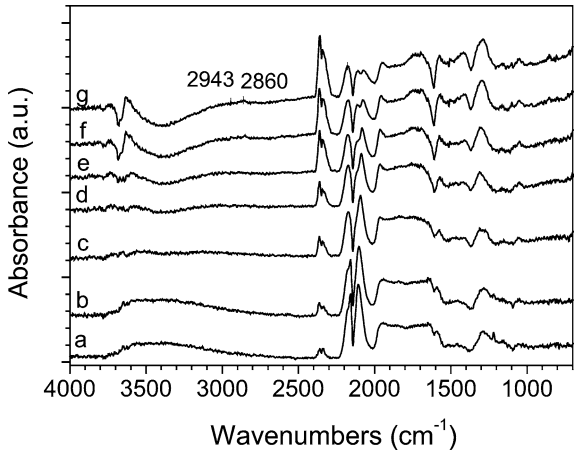

Fig. 8. DRIFTS of CO adsorption in 5% CO/Ar flow on Pd/CeO_2 at (a) 25 °C, (b) 50 °C, (c) 100 °C, (d) 150 °C, (e) 200 °C, (f) 250 °C, and (g) 300 °C.

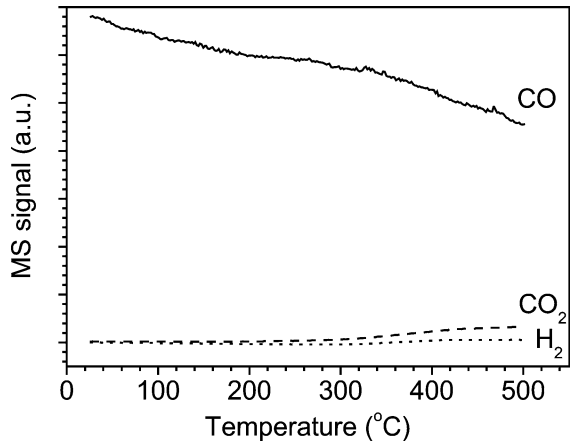

Fig. 9. CO-TPR profiles of the calcined TiO_2.

mation as shown in Fig. 9, indicating the occurrence of the WGS reaction. The production of CO_2 cannot be attributed to the reduction of TiO_2 at such a low temperature as proved by H_2-TPR measurement. Therefore, the CO_2 evolved seems to be only from the WGS reaction between the CO and the surface hydroxyl groups in the sample.

For Pd/TiO_2, CO_2 alone is produced as soon as the CO/Ar flow was switched into the system as shown in Fig. 6, indicating that the reduction of PdO species occurs at ambient temperature. Further increase of temperature leads to a further release of CO_2 alone with the apex around 170 °C and the amounts of CO_2 evolved correspond almost with the stoichiometrical CO consumption (see Fig. 10). This peak should be also assigned to the reduction of PdO, because TiO_2 cannot be reduced at this temperature. As shown in Table 2, the amounts of CO_2 evolved at ambient temperature and thereafter up to 214 °C (the peak with the apex around 170 °C) is 18 and 64 μmol/g, respectively. Because the CO_2 production corresponding to a complete reduction of PdO is 94 μmol/g, only 19% PdO is reduced under ambient temperature and 68% is reduced during the CO-TPR at low temperature.

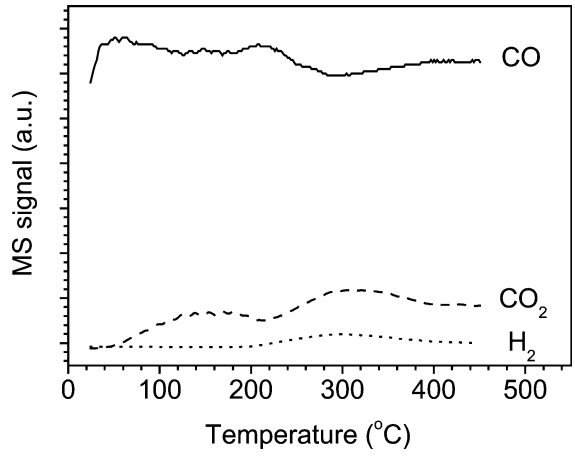

Fig. 10. CO-TPR profiles of the calcined Pd/TiO_2.

However, the DRIFTS of CO adsorption at room temperature revealed that only metallic Pd is detected. Tessier et al. [54] showed that PdO in Pd/Al_2O_3 could be partially reduced to metallic Pd by CO at room temperature to form an outer palladium layer around the core of palladium oxide. The reduction of Pd/TiO_2 may be similar to the case of Pd/Al_2O_3. Only the outermost layer of the PdO cluster contacted directly with CO can be reduced at room temperature. The formation of CO_2 at ambient temperature is related to the reduction of the outermost layer of PdO and that at higher temperature may be ascribed to the further reduction of core PdO.

A second band of CO consumption starts at 214 °C and peaks at about 305 °C accompanied with the production of CO_2 and H_2, which may be ascribed to the WGS reaction between adsorbed CO and the hydroxyl groups in the support. CO disproportionation is also excluded by the successive O_2-TPO. Compared to the case of individual TiO_2, the presence of Pd enhances the WGS reaction greatly.

The DRIFTS of CO adsorption on Pd/TiO_2 in CO/Ar flow at different temperatures are shown in Fig. 11. It is noted that the saturated adsorption of CO at room temperature causes the absorbance of gaseous CO_2 (2400–2300 cm^{-1}). The linear adsorption of CO on Pd^0 (2085 cm^{-1}) is overlapped by the absorption of gaseous CO (2175 and 2120 cm^{-1}). No evident absorption is detected in the carbonate region (1800–800 cm^{-1}). As the temperature increased, the free water appeared at 3720 cm^{-1} accompanied with the occurrence of bicarbonate species adsorbed on Ti ions at 859 cm^{-1}. When the temperature increased to 100 °C, the bands 1504, 1442, 1341, and 1220 cm^{-1} ascribed to carbonate-like species adsorbed on titania are detected [55]. Meanwhile, the intensity of free water increased and the negative bands at 3635 cm^{-1} assigned to the OH groups on Ti ions are observed. Above 250 °C, the free water disappears and the decrease of OH group is more evident. Because TiO_2 cannot be reduced at the relative low temperature, the WGS reaction between CO

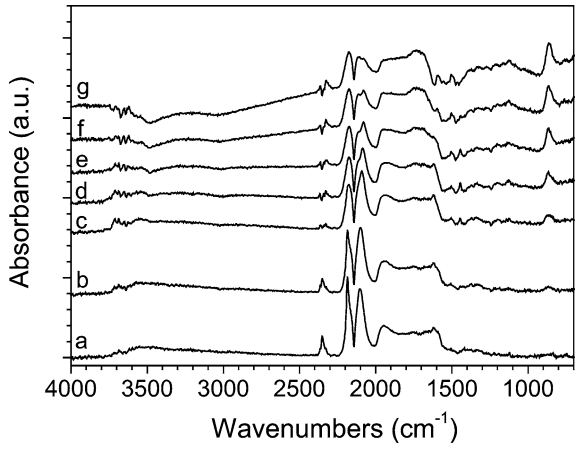

Fig. 11. DRIFTS of CO adsorption in 5% CO/Ar flow on Pd/TiO_2 at (a) 25 °C, (b) 50 °C, (c) 100 °C, (d) 150 °C, (e) 200 °C, (f) 250 °C, and (g) 300 °C.

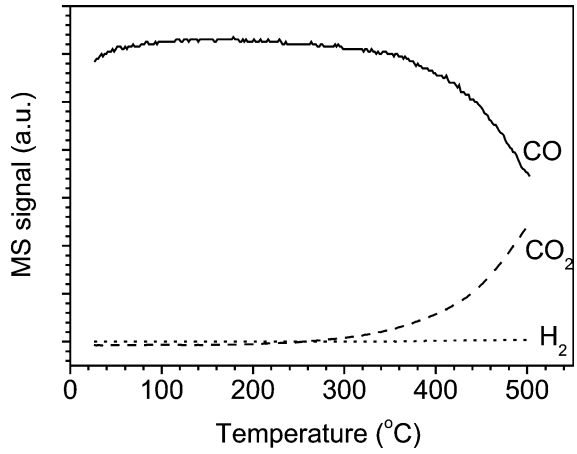

Fig. 12. CO-TPR profiles of the calcined CeO_2–TiO_2.

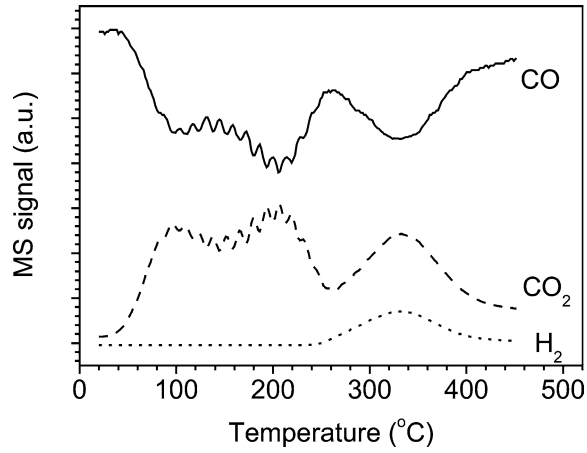

Fig. 13. CO-TPR profiles of the calcined Pd/CeO_2–TiO_2.

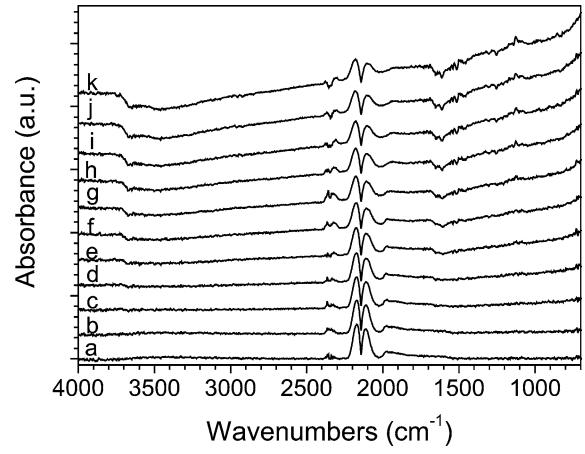

Fig. 14. DRIFTS of CO adsorption in 5% CO/Ar flow on Pd/CeO_2–TiO_2 at (a) 25 °C, (b) 50 °C, (c) 100 °C, (d) 150 °C, (e) 200 °C, (f) 250 °C, (g) 300 °C, (h) 350 °C, (i) 400 °C, (j) 450 °C, and (k) 500 °C.

and OH groups on TiO_2 may follow the associative mechanism with the formate or bicarbonate species as intermediates.

3.5.3. *CeO_2–TiO_2 and Pd/CeO_2–TiO_2*

For CeO_2–TiO_2, the consumption of CO starts at around 300 °C accompanied by the production of CO_2 (see Fig. 12). H_2 is not detected, indicating that the WGS reaction is negligible for the CO-TPR of CeO_2–TiO_2 at the temperature investigated here. The CO consumption and CO_2 production should be attributed to the reaction between CO and the surface oxygen in CeO_2–TiO_2. Compared with the individual CeO_2, the initial reduction temperature and peak position shift to higher temperatures, indicating that the reduction of CeO_2–TiO_2 becomes much more difficult, just as suggested by the results of H_2-TPR measurement.

For Pd/CeO_2–TiO_2 as shown in Fig. 6, a large quantity of CO_2 is released after being switched to a CO/Ar atmosphere, indicating that a remarkable reduction takes place at ambient temperature. The CO_2 evolved in this stage is 123.2 μmol/g, which is markedly larger than the amount of CO_2 produced from the reduction of PdO alone in the sample. This may imply that the reduction of PdO is fully achieved; moreover, part of CeO_2 in the sample is also reduced at ambient temperature.

With the increase of temperature (see Fig. 13), CO_2 production shows three main peaks at 95, 205, and 330 °C, respectively, which were accompanied by nearly stoichiometrical CO consumption. H_2 production is detected at 240 °C and shows a peak at 330 °C. As discussed above, these peaks should be ascribed to the reduction of surface oxygen in CeO_2–TiO_2 support, which results in the formation of various nonstoichiometric cerium oxide species. The third peak is also partially ascribed to the WGS between the adsorbed CO and the hydroxyl groups.

The DRIFTS of CO adsorption on Pd/CeO_2–TiO_2 in CO/Ar flow at different temperatures are shown in Fig. 14. The absorbance of gaseous CO_2 in 2400–2300 cm^{-1} is also detected at room temperature. The linear adsorption of CO on Pd^0 (2089 cm^{-1}) is overlapped by the absorption of gaseous CO (2175 and 2120 cm^{-1}). No evident absorbance is detected in the carbonate region (1800–800 cm^{-1}). The

negative bands in 3400–3800 cm^{-1} corresponding to the hydroxyl are detected with the increase of temperature. Only a band at 1120 cm^{-1} is observed in the carbonates region, which is ascribed to the bridged carbonate according to the assignment of Holmgren et al. [53]. Therefore, the WGS reaction between adsorbed CO and the hydroxyl groups on ceria may proceed through the redox mechanism,

$$CO(ads) + 2CeO_2 = CO_2 + Ce_2O_3,$$
$$OH + Ce_2O_3 = 2CeO_2 + \tfrac{1}{2}H_2,$$

where CeO_2 is reduced to Ce_2O_3 by CO to give CO_2 and the hydroxyl group then react with Ce_2O_3 to give CeO_2 and H_2.

In comparison with Pd/CeO_2, the reduction temperature of PdO–CeO_2 interface species in Pd/CeO_2–TiO_2 decreased. Although the mixed CeO_2–TiO_2 support is more difficult to be reduced than the individual CeO_2, the presence of Pd changes such a situation; i.e., CeO_2 in Pd/CeO_2–TiO_2 becomes more easily reduced than that in Pd/CeO_2. As shown in Table 2, the easily reducible CeO_2 by CO in Pd/CeO_2 is 26%, while 96% of CeO_2 in Pd/CeO_2–TiO_2 is reduced in the CO-TPR process. The reduction of PdO and interfacial CeO_2 in Pd/CeO_2–TiO_2 becomes much easier than that in Pd/CeO_2 due to the special Pd–Ce–Ti interaction, which may contribute to the high activity for the CO oxidation at low temperatures [31]. The interaction between Pd and supports has an effect on the adsorption properties of CO, which may indicate the different electronic effects in the catalysts. On the other hand, the geometric effects also play an important role for the Pd–support interactions, the variance of the reducibility may be caused by the different locations of Pd on the supports or the different orientations of Pd combination to the supports. The special Pd–Ce–Ti interaction in Pd/CeO_2–TiO_2 may be originated from both the electronic effect that affects the CO adsorption and the geometric effect that may contribute to the reducibility variance of PdO. However, such assumptions should be confirmed by the further works such as XPS and HREM characterization.

4. Conclusions

The catalysts Pd/TiO_2, Pd/CeO_2, and Pd/CeO_2–TiO_2 for the CO oxidation at low temperatures together with their corresponding supports were characterized by means of N_2 adsorption, XRD, DRIFTS, H_2-TPR, and CO-TPR. The characteristics and reducibility of Pd and other active species involved in CO oxidation were then investigated. The results showed that PdO is finely dispersed on the supports with high surface area. DRIFTS of CO adsorption further indicated that both Pd^{2+} and Pd^0 species coexist in Pd/CeO_2, while only Pd^0 is detected in Pd/TiO_2 and Pd/CeO_2–TiO_2.

H_2-TPR showed that no bulk CeO_2 exists in CeO_2–TiO_2 and the reduction of CeO_2–TiO_2 is more difficult than that of the individual CeO_2. PdO in Pd/TiO_2 can be fully reduced by H_2 at ambient temperature, whereas PdO in Pd/CeO_2 and Pd/CeO_2–TiO_2 is reduced respectively at 162 and 80 °C, accompanied by the partial reduction of CeO_2.

CO-TPR showed that the reduction of PdO over TiO_2 by CO is limited within the outermost layer at ambient temperature and the core PdO can be reduced further with the increase of temperature. PdO/CeO_2 is also reduced both at ambient temperature and with the increase of temperature during the CO-TPR process; and the reduction temperature of CeO_2 decreased significantly with the presence of PdO. The reducibility variance of PdO in Pd/CeO_2 catalyst may be due to the different locations of PdO on CeO_2. A complete reduction of PdO in Pd/CeO_2–TiO_2 by CO is achieved at ambient temperature, accompanied by the partial reduction of CeO_2, which may indicate that the special Pd–Ce–Ti interaction in Pd/CeO_2–TiO_2 is favorable for the reduction of PdO and interfacial CeO_2 species. This may contribute to the high activity for the CO oxidation at low temperature. The special Pd–Ce–Ti interaction in Pd/CeO_2–TiO_2 may be originated from both the electronic effect that affects the CO adsorption and the geometric effect that may contribute to the reducibility variance of PdO.

Both H_2-TPR and CO-TPR proved that the reduction of CeO_2–TiO_2 is more difficult than that of the surface oxygen in the individual CeO_2 probably due to the formation of CeO_2–TiO_2 solid solution. However, the addition of PdO changes the situation: the reduction of Pd/CeO_2–TiO_2 becomes much easier than that of Pd/CeO_2.

The WGS between CO and the hydroxyl groups in the catalysts is detected at a temperature higher than 210 °C during the CO-TPR process on all of the Pd supported catalysts as well as the individual CeO_2 and TiO_2 supports. Moreover, the WGS in the CO-TPR for various catalysts may be different in the reaction mechanism, and the presence of Pd is favorable for the WGS reaction.

Acknowledgments

The authors are grateful for the financial supports of the Natural Science Foundation of Shanxi Province (No. 20011020) and the State Key Fundamental Research Project of China.

References

[1] M. Haruta, N. Yamada, T. Kobayashi, S. Iijima, J. Catal. 115 (1989) 301.
[2] M. Haruta, S. Tsubota, T. Kobayashi, H. Kageyama, M.J. Genet, B. Delmon, J. Catal. 144 (1993) 175.
[3] Y. Iizuka, T. Tode, T. Takao, K.L. Yatsu, T. Takeuchi, S. Tsubota, M. Haruta, J. Catal. 187 (1999) 50.
[4] M. Haruta, Catal. Today 36 (1997) 153.
[5] P. Bera, M.S. Hegde, Catal. Lett. 79 (2002) 75.
[6] W. Liu, M. Flytzani-Stephanopoulos, J. Catal. 153 (1995) 317.
[7] D.R. Schryer, B.T. Upchurch, J.O. van Norman, K.G. Brown, J. Schryer, J. Catal. 122 (1990) 193.

[8] S.E. Golunski, H.A. Hatcher, R.R. Rajaram, T.J. Truex, Appl. Catal. B 5 (1995) 367.
[9] D.I. Kochubey, S.N. Pavlova, B.N. Novgorodov, G.N. Kryukova, V.A. Sadykov, J. Catal. 161 (1996) 500.
[10] S.N. Pavlova, V.A. Sadykov, V.A. Razdobarov, E.A. Paukshtis, J. Catal. 161 (1996) 507.
[11] S.N. Pavlova, V.A. Sadykov, N.N. Bulgakov, M.N. Bredikhin, J. Catal. 161 (1996) 517.
[12] M.F. Luo, Z.Y. Hou, X.X. Yuan, X.M. Zheng, Catal. Lett. 50 (1998) 205.
[13] R.A. Searles, Stud. Surf. Sci. Catal. 116 (1998) 23.
[14] S.J. Tauster, S.C. Fung, R.L. Garten, J. Am. Chem. Soc. 100 (1978) 170.
[15] S. Bernal, J.J. Calvino, M.A. Cauqui, J.M. Gatica, C. Larese, J.A. Pérez Omil, J.M. Pintado, Catal. Today 50 (1999) 175.
[16] J. Evans, B.E. Hayden, G. Lu, Surf. Sci. 360 (1996) 61.
[17] G.S. Lane, E.E. Wolf, J. Catal. 105 (1987) 386.
[18] S. Tsubota, D. Cunningham, Y. Bando, M. Haruta, Stud. Surf. Sci. Catal. 77 (1993) 325.
[19] A. Trovarelli, Catal. Rev.-Sci. Eng. 38 (1996) 439.
[20] J. Kašpar, P. Fornasiero, M. Graziani, Catal. Today 50 (1999) 285.
[21] M. Fernández-García, A. Martínez-Arias, L.N. Salamanca, J.M. Coronado, J.A. Anderson, J.C. Conesa, J. Soria, J. Catal. 187 (1999) 474.
[22] T. Jin, T. Okuhara, G.J. Mains, J.M. White, J. Phys. Chem. 91 (1987) 3310.
[23] G.S. Zafiris, R.J. Gorte, J. Catal. 139 (1993) 561.
[24] H. Cordatos, R.J. Gorte, J. Catal. 159 (1996) 112.
[25] S.H. Oh, C.C. Eickle, J. Catal. 112 (1988) 543.
[26] G.S. Zafiris, R.J. Gorte, J. Catal. 143 (1993) 86.
[27] T. Bunluesin, H. Cordatos, R.J. Gorte, J. Catal. 157 (1995) 222.
[28] T. Bunluesin, E.S. Putna, R.J. Gorte, Catal. Lett. 41 (1996) 1.
[29] T. Bunluesin, G.W. Graham, R.J. Gorte, Appl. Catal. B 14 (1997) 105.
[30] T. Bunluesin, R.J. Gorte, G.W. Graham, Appl. Catal. B 15 (1998) 107.
[31] G.L. Dong, J.G. Wang, Y.B. Gao, S.Y. Chen, Catal. Lett. 58 (1999) 37.
[32] H.P. Klug, L.E. Alexander, X-Ray Diffraction Procedures, Wiley, New York, 1967.
[33] G.L. Dong, J.G. Wang, Y.B. Gao, S.Y. Chen, J. Inorg. Mater. (Chinese) 14 (1999) 873.
[34] M.G. Sanchez, J.L. Gazquez, J. Catal. 104 (1987) 120.
[35] A. Dauscher, P. Wehrer, L. Hilaire, Catal. Lett. 14 (1992) 171.
[36] M.F. Luo, J. Chen, L.S. Chen, J.Q. Lu, Z.C. Feng, C. Li, Chem. Mater. 13 (2001) 197.
[37] J. Rynkowski, J. Farbotko, R. Touroude, L. Hilaire, Appl. Catal. A 203 (2000) 335.
[38] M. Fernández-García, A. Martínez-Arias, A. Iglesias-Juez, A.B. Hungría, J.A. Anderson, J.C. Conesa, J. Soria, Appl. Catal. B 31 (2001) 39.
[39] A. Martínez-Arias, M. Fernández-García, A. Iglesias-Juez, A.B. Hungría, J.A. Anderson, J.C. Conesa, J. Soria, Appl. Catal. B 31 (2001) 51.
[40] K.I. Choi, M.A. Vannic, J. Catal. 127 (1991) 465.
[41] A. Bensalem, J.C. Muller, D. Tessier, F. Bozon-Verduraz, J. Chem. Soc., Faraday Trans. 92 (1996) 3233.
[42] T. Tabakova, F. Boccuzzi, M. Manzoli, D. Andreeva, Appl. Catal. A 252 (2003) 385.
[43] S. Hilaire, X. Wang, T. Luo, R.J. Gorte, J. Wagner, Appl. Catal. A 215 (2001) 271.
[44] H.C. Yao, Y.F. Yu Yao, J. Catal. 86 (1984) 254.
[45] F. Giordano, A. Trovarelli, C. de Leitenburg, M. Giona, J. Catal. 193 (2000) 273.
[46] H. Cordatos, T. Bunluesin, J. Stubenrauch, J.M. Vohs, R.J. Gorte, J. Phys. Chem. 100 (1996) 785.
[47] H.W. Jen, G.W. Graham, W. Chun, R.W. McCabe, J.P. Cuif, S.E. Deutsch, O. Touret, Catal. Today 50 (1999) 309.
[48] C. Serre, F. Garin, G. Belot, G. Maire, J. Catal. 141 (1993) 1.
[49] A. Martínez-Arias, J.M. Coronado, R. Cataluna, J.C. Conesa, J. Soria, J. Phys. Chem. B 102 (1998) 4357.
[50] T. Shido, Y. Iwasawa, J. Catal. 141 (1993) 71.
[51] T. Shido, K. Asakura, Y. Iwasawa, J. Catal. 122 (1990) 55.
[52] G. Jacobs, L. Williams, U. Graham, D. Sparks, B.H. Davis, J. Phys. Chem. B 107 (2003) 10398.
[53] A. Holmgren, B. Andersson, D. Duprez, Appl. Catal. B 22 (1999) 215.
[54] D. Tessier, A. Rakai, F. Bozon-Verduraz, J. Chem. Soc., Faraday Trans. 88 (1992) 741.
[55] F. Boccuzzi, A. Chiotino, J. Phys. Chem. 100 (1996) 3617.